A fast-responding CO_2 microelectrode for profiling sediments, microbial mats, and biofilms

Dirk de Beer, Anni Glud, Eric Epping, and Michael Kühl

Max Planck Institute for Marine Microbiology, Microsensor Research Group, Celsiusstrasse 1, D-28359 Bremen, Germany

Abstract

A new CO_2 microelectrode with a tip diameter of 10 μm and a response time (t_{90}) of ~10 s is presented. The sensor allows CO_2 measurements with a detection limit of <3 μM. The microsensor was tested in experimental systems of increasing complexity. A diffusion-reaction simulation model was used to calculate CO_2 profiles in order to check the reliability of the measured profiles. Measured CO_2 and O_2 profiles showed that, in highly active layers with photosynthetic and respiratory organisms, local equilibrium of the carbonate system cannot be assumed. In such highly active systems, the CO_2 profiles were determined by the slow CO_2 hydration rate, the biological conversion rates, and the diffusion of all species of the carbonate system. We concluded that measured CO_2 profiles cannot easily be extrapolated to describe the total carbonate concentration profile, because CO_2 may not be in equilibrium with the rest of the carbonate system, and because a very accurate alignment of pH and CO_2 profiles is needed to calculate C_T. However, the new CO_2 microelectrode is useful in research involving biological processes directly producing or consuming CO_2 such as photosynthesis or respiration.

The carbonate system plays a central role in aquatic biological processes, as CO_2 is released by respiration and consumed by photosynthesis. Furthermore, the carbonate system is involved in the diagenesis of calcite and aragonite. The distribution of dissolved inorganic carbon (DIC) species determines and reflects both the presence and magnitude of these processes. Consequently, determination of total DIC (C_T) profiles has been given considerable attention (Canfield et al. 1993; Cai and Reimers 1993). In sediments, C_T profiles have mostly been determined by pore-water analysis. However, in sediments with high rates of CO_2 production or consumption, such pore-water analyses may have insufficient spatial resolution, and the technique is not practical in biofilms (often <1 mm in thickness). Furthermore, collection of pore water may change its composition (Bender et al. 1987). In situ determination of the carbonate system with microsensors can circumvent these problems.

Some sensors are presently available for pH, CO_3^{2-}, and CO_2. Carbonate liquid membrane sensors have been described by Herman and Rechnitz (1974). However, for environmental studies detection limits of sensors are a problem, and CO_3^{2-} sensors cannot be used in seawater. The concept of CO_2 sensors is based on a CO_2-induced pH change of an electrolyte separated from the sample by a gas-permeable membrane (Severinghaus and Bradley 1958). Cai and Reimers (1993) prepared and used a sturdy CO_2 sensor with a tip size of 300 μm. This size allows profiling of relatively gradual CO_2 profiles, such as in deep-sea sediments. However, in many systems, the most active layers are 100–1,000 μm thick, for which a smaller sensor is needed. Our aim was to develop a CO_2 microsensor with a tip diameter of a few micrometers.

Materials and methods

Microelectrodes—pH microsensor. Solidified neutral carrier-based liquid ion-exchange membrane (LIX) pH microelectrodes (Lee and de Beer 1995) were used both as the internal sensor in the CO_2 microsensor and for pH profiling. Green soda lime glass tubes (8516, Schott) were drawn into microcapillaries with a tip diameter of 3–5 μm by using a heating coil. After pulling, the glass surface of the capillaries was silanized, according to Amman et al. (1987), however, with longer preincubation (3 h 150°C) and reaction times (overnight, 200°C).

Two types of liquid ion-exchange membrane (LIX) solutions were used. Type 1 was a solution of 6% (wt/wt) 4-nonadecylpyridine (H+ Ionophore II, ETH1907) and 1% (wt/wt) potassium tetrakis(4-chlorophenyl)borate in 2-nitrophenyl octyl ether. Type 2 was a solution of 3% (wt/wt) N,N-dioctadecylmethylamine (H+ Ionophore III) and 1% (wt/wt) sodium tetraphenyl borate in 2-nitrophenyl octyl ether. From each type of LIX a portion was taken to which 10% (wt/wt) high-MW poly(vinylchloride) was added. Then, ~3 volumes of tetrahydrofuran (Fluka, Selectophor quality) were added to the mixture to dissolve the PVC. According to the manufacturer's specifications, the usable measuring range of type 1 is from pH 2 to 9.5, and of type 2 from pH 3 to 11. All LIX components and the silanizing agent were obtained from Fluka. The silanized capillaries were filled with electrolyte, and a solidified membrane was brought in the tip, as described previously (Lee and de Beer 1994).

The pH sensors for use in CO_2 sensors were made slender with a taper at the tip of ~5°, while an angle of ~10° made the profiling pH sensors more sturdy. In addition, the sensors for pH profiling were electrically shielded as described by
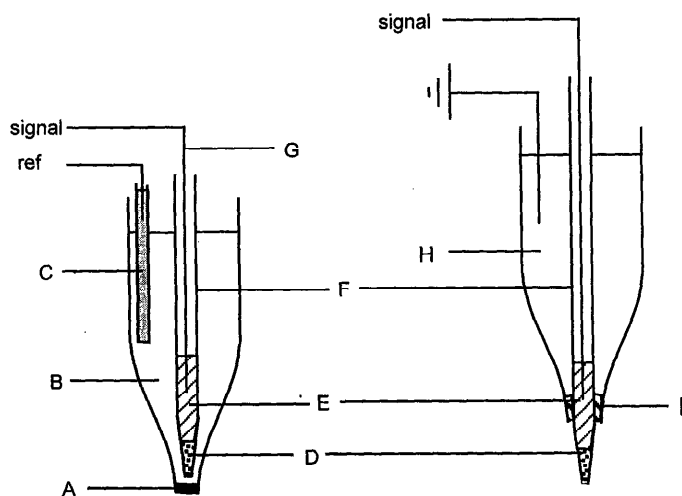
Fig. 1. Design of the CO_2 (left) and pH (right) microsensors. (A) Silicon membrane, (B) electrolyte 2, (C) reference electrode, (D) LIX membrane, (E) electrolyte 1, (F) pH microsensor, (G) shielded Ag/AgCl wire, (H) 3 M KCl, and (I) silicon kit to fixate shielding.

Jensen et al. (1993) (Fig. 1). Because of its higher pH range, LIX type 2 was used in photosynthesis experiments. Calibration of the microelectrodes was performed according to Lee and de Beer (1995) or with standard pH solutions. The slope of the calibrations was between 54 and 58 mV per pH

Table 1. Numerical values of used constants.

K_1 (seawater)	9.33×10^{-7}*
K_2 (seawater)	6.61×10^{-10}*
K_1 (freshwater)	4.46×10^{-7}†
K_2 (freshwater)	5.01×10^{-11}†
k_1	0.0217 liter s^{-1}‡
k_2	13.977 liter s^{-1}‡
k_3	8.2×10^3 mol liter^{-1} s^{-1}§
k_4	8.3×10^{-4} liter s^{-1}§
Respiration	
$K_m(O_2)$	0.35 μM‖
Photosynthesis	
$K_m(CO_2)$	0.0019 μM#
K_m (HCO$_3^-$)	100 μM¶,**
Diffusion coefficients	
HCO$_3^-$	9.6×10^{-10} m^2 s^{-1}††
CO$_3^{-2}$	7.8×10^{-10} m^2 s^{-1}‡‡
H$_2$CO$_3$	1×10^{-9} m^2 s^{-1}
CO$_2$	1.75×10^{-9} m^2 s^{-1}††
O$_2$	2×10^{-9} m^2 s^{-1}

* Mehrbach et al. 1973.
† Stumm and Morgan 1981.
‡ Portielje and Lijklema 1995.
§ Johnson 1982.
‖ Gerritse et al. 1992.
Aizawa and Miyachi 1986.
¶ Ludden et al. 1985.
** Kaplan et al. 1994.
†† Li and Gregory 1974.
‡‡ Shanagan and Ho 1986.

Notations

C	Concentration (mol m^{-3})
C_T	Total dissolved inorganic carbon (mol m^{-3})
C_{Td}	C_T calculated with reaction diffusion model (mol m^{-3})
C_{Te}	C_T calculated from CO$_2$ and pH profiles assuming local equilibrium (mol m^{-3})
D	Diffusion coefficient (m^2 s^{-1})
DIC	Dissolved inorganic carbon
E	Sensor signal (mV)
i	Iteration step index
J	Flux (mol m^{-2} s^{-1})
H	Dimensionless vapor/waterphase distribution coefficient ($-/-$)
K_m	Saturation constant (mol m^{-3})
$k_{1,2}$	Rate constants for hydration reaction 1 (1 s^{-1})
$k_{3,4}$	Rate constants for reaction 2 (m^3 mol^{-1} s^{-1})
$K_{1,2}$	Equilibrium constants carbonate system
$K(H_2CO_3)$	Equilibrium constant H$_2$CO$_3$ dissociation
n	Layer index number
P	Volumetric photosynthetic activity (mol m^{-3} s^{-1})
P_{max}	Maximal volumetric photosynthetic activity (mol m^{-3} s^{-1})
R	Volumetric respiratory activity (mol m^{-3} s^{-1})
R_{max}	Maximal volumetric respiratory activity (mol m^{-3} s^{-1})
ΣV_C	Net conversion rate of carbon species (mol m^{-3} s^{-1})
t	Time (s)
x	Position (m)
X_{1-3}	Constants used in calibration equation ($-$)

unit. The response time (t_{90}, the time needed to reach 90% of the end value upon a concentration change) was <5 s after a pH step of 3 units.

CO₂ microsensor. The CO$_2$ microsensor consisted of an outer glass casing sealed at the tip with a silicon membrane and containing a pH microsensor positioned close to the membrane (Fig. 1). Casings were prepared with a tip size of ~10 μm from Pasteur pipettes (Revsbech 1989). The tip was sealed with a silicon membrane (Dispersion Coating 92-009, Dow Corning) that had a maximum thickness of 5 μm and was cured overnight. The silicon used has been reported as highly CO$_2$ permeable (Goyet et al. 1992).

The tips of the casings were filled with electrolyte 2, a solution of 1 mM NaHCO$_3$, 150 mM NaCl, 0.5% carbonic anhydrase (from bovine erythrocytes, Sigma), and 35 mg liter^{-1} chloramphenicol (Sigma). The pH sensor was inserted into the casing, and the tip was positioned at a distance of 3–10 μm from the silicon membrane. The pH sensor was glued to the outer casing with a drop of cyanoacrylic glue, left for 20 min, and further glued with two-component epoxy glue (Super Epoxy, AB Hisingeplast), and left for 1 h. The epoxy glue shrinks slightly, and if applied without previous fixation with cyanoacrylic glue, the pH sensor will be displaced and broken. Cyanoacrylate is sensitive to moisture; thus, without additional application of the two-component glue, the pH sensor may loosen. Finally, the casings were almost completely filled with electrolyte 2, but contact with the glue was avoided. The electrolyte in the pH sensor was connected with an Ag/AgCl wire to the input of an amplifier,
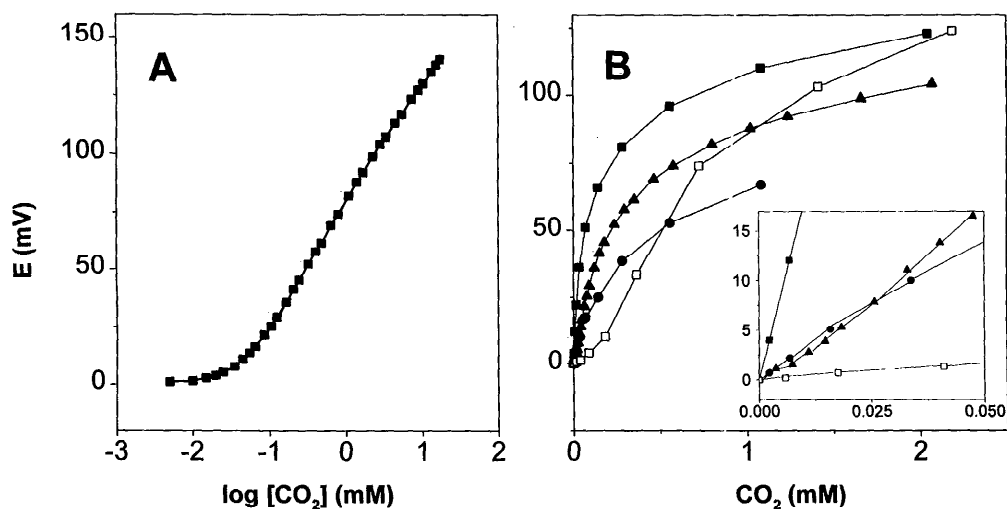
Fig. 2.   (A) Calibration curve of a CO_2 microsensor with loose fit between the internal pH sensor and the outer casing. The signal is plotted vs. the logarithm of the CO_2 concentration. (B) The same for sensors of different design, with the signal plotted directly against the CO_2 concentration. The fit between pH sensor and casing was close (■—■), loose (▲—▲, ●—●); □—□ represents a sensor with a loose fit and without carbonic anhydrase. The insert shows a magnification of Fig. 2B at low CO_2 concentrations.

while an agar salt-bridge connected electrolyte 2 with a Ag/AgCl reference. After connection, the electrodes were left in degassed solution until the signal was constant.

The CO_2 sensor was calibrated at experimental temperature in 50 mM phosphate buffer (pH 7.2). The buffer was degassed by boiling and cooling under vacuum and then purged with N_2 for 10 min. The CO_2 concentration was increased stepwise by adding aliquots of a carbonate solution, consisting of 200 mM Na_2CO_3 and 50 mM phosphate buffer (pH 7.2). CO_2 concentrations were calculated from freshwater equilibrium constants (Table 1) and corrected with activity coefficients from the Güntelberg approximation (Stumm and Morgan 1981). Calibrations were made before and after each series of experiments, typically every 2 h, and this procedure could be completed in as little as 10 min.

Oxygen microsensor. Clark-type O_2 microsensors with internal reference and guard cathode were prepared and calibrated as described previously by Revsbech (1989). Their stirring sensitivity was <2%.

The microsensors were mounted on a micromanipulator for microprofile measurements. The position relative to the solid surface was determined visually using a dissection microscope.

Experimental set-up—Abiotic model system. A diffusion cell was used to create nonbiogenic CO_2 profiles in an agar gel. A 3–5-mm-thick agar membrane (2% wt/vol in distilled water) was placed between two electrolytes in a 250-ml top and a 300-ml bottom chamber. By varying the pH and C_T concentrations in the top and bottom volumes, different CO_2 profiles developed in the agar slab. Measurements were done after 24 h of incubation. The liquid residence time in the chambers was 10 min. The bottom chamber was stirred with a magnetic stirrer, the top with an impeller. The exchange surface was circular and had a diameter of 1 cm. A CO_2 and

a pH microelectrode were mounted in parallel on one micromanipulator. The distance between the sensor tips was ~1 mm. Both tips were adjusted flush with the water surface. Profiles were measured within 2 mm of the center of the agar membrane. The tips penetrated the agar simultaneously, and because of the absence of lateral gradients, the measured profiles could be directly compared.

Biotic model system. Photosynthetic cyanobacteria (*Synechococcus* MPI[SAG1402-1]95-1) and respiratory bacteria (*Comamonas testosteroni* DSM 50244) were immobilized in an agar gel. The strains were immobilized either in different gels or in one gel system, but were spatially separated. A culture of *C. testosteroni* was concentrated by centrifugation and immobilized in 1.4% agarose slabs of ~1-cm thickness. A suspension of the *Synechococcus* cells in unsolidified agarose was poured to 1-mm thickness on top of the *C. testosteroni*-containing gels. The gels were left 2 h at 20°C in darkness before microprofile measurements were started. Profiles in light were recorded after 2 h of illumination.

Sediments. Silty and sandy sediment cores, with a diameter of 6 cm, were taken (November 1995) from an intertidal mud flat of the Weser Estuary, Germany. The cores were covered with 4 cm of water from the same site (salinity 2.5‰) and incubated in the dark at 20°C. The liquid was agitated by blowing a water-saturated airstream over the surface. After 3 d, O_2, pH, and CO_2 microprofiles were measured. In one of the experiments pore water was extracted by a sediment squeezer (Bender et al. 1987) after recording the microprofiles. Pore-water samples (0.5 ml) were preserved with 5 µl saturated $HgCl_2$ and stored at 4°C. C_T in the pore water was determined within 1 week after sampling using flow injection analysis (Hall and Aller 1992).

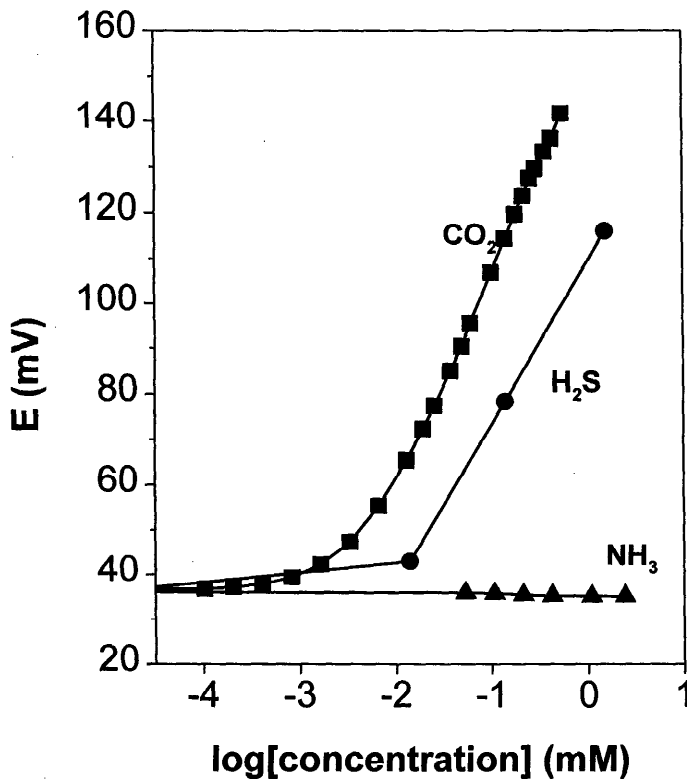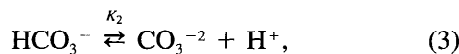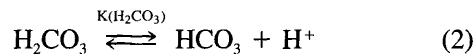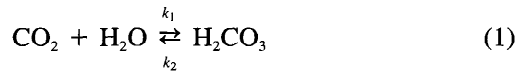*Modeling profiles*—The carbonate system species are related by the following reactions:

Fig. 3. Effect of H$_2$S (●—●) and NH$_3$ (▲—▲) on the signal of a CO$_2$ microsensor with a loose fit, as compared to its response to CO$_2$ (■—■).

$$CO_2 + H_2O \overset{k_1}{\underset{k_2}{\rightleftarrows}} H_2CO_3 \tag{1}$$

$$H_2CO_3 \overset{K(H_2CO_3)}{\rightleftarrows} HCO_3^- + H^+ \tag{2}$$

$$HCO_3^- \overset{K_2}{\rightleftarrows} CO_3^{-2} + H^+, \tag{3}$$

where the lower and upper case *k*s are kinetic and thermodynamic constants, respectively. The hydration of CO$_2$ (Eq. 1) is rather slow but can be catalyzed (e.g. by the enzyme carbonic anhydrase). Reactions 2 and 3 are fast and equilibrium is usually assumed to be reached instantaneously (Ho and Shanahan 1986). CO$_2$ can also react with OH$^-$ to form HCO$_3^-$ directly:

$$CO_2 + OH^- \overset{k_3}{\underset{k_2}{\rightleftarrows}} HCO_3^-. \tag{4}$$
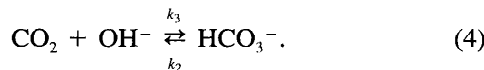
This reaction is of increasing importance at higher pH, and above pH 8.7 it is faster than reaction 1.

At equilibrium, the relative concentrations of CO$_2$, H$_2$CO$_3$, HCO$_3^-$, and CO$_3^{2-}$ depend on the pH. The carbonate system is in equilibrium if the thermodynamic constants can be used to describe the local concentrations of all carbonate species at the local pH. Steady state occurs when no temporal concentration changes take place, i.e. the diffusional transport rate equals the local reaction rate of the CO$_2$ hydration/dehydration and biological conversions. Because the noncata-

lyzed hydration of CO$_2$ to H$_2$CO$_3$ is slow, the carbonate system is out of equilibrium if CO$_2$ is rapidly produced or consumed. In a steep C_T gradient, local CO$_2$ concentrations may be out of equilibrium, even in a steady-state situation, because the diffusivities of the carbonate species are different. If biological reactions also occur, profiles of CO$_2$, H$_2$CO$_3$, HCO$_3^-$, CO$_3^-$, and O$_2$ are determined by three processes: (1) equilibrium reactions with the carbonate system, (2) biological production or consumption, and (3) diffusional transport. A reaction-diffusion model is then needed to interpret measured CO$_2$ profiles in relation to the carbonate system and local conversions.

The reactions considered were: respiration, resulting in the stoichiometric conversion of oxygen to carbon dioxide; photosynthesis, the stoichiometric conversion of carbon dioxide and bicarbonate to oxygen; CO$_2$ hydration (Eq. 1 and 4) and the carbonate equilibria (Eq. 2 and 3). Monod kinetics were used for respiration:

$$R = R_{max}\frac{S}{K_m + S}, \tag{5a}$$

where R is the respiration rate, R_{max} the maximal respiration rate, and K_m the half-saturation constant for oxygen. Photosynthesis was described as

$$P = P_{max}\frac{S}{K_m + S}, \tag{5b}$$

where P is the photosynthesis rate, P_{max} the maximal photosynthesis rate, and K_m the half-saturation constant for CO$_2$ and(or) HCO$_3^-$.

The sediment or mat is divided into a number of hypothetical layers. In each layer the concentration changes (of dissolved inorganic carbon and O$_2$), during an interval, due to diffusion and conversion are calculated from an explicit difference scheme (Pearson 1986):

$$\Delta C_{n,i} = \Delta t\left[\frac{D}{\Delta x}\left(\frac{C_{n+1,i} - C_{n,i}}{\Delta x} - \frac{C_{n,i} - C_{n-1,i}}{\Delta x}\right) - \Sigma V_c\right] \tag{6}$$

and

$$C_{n,i+1} = C_{n,i} + \Delta C_{n,i}, \tag{7}$$

where C is the concentration, n is the layer index, i the time-step index, D the diffusion coefficient, Δx the position increment, Δt the length of the time step, and ΣV_c the net conversion, including biological consumption and production, as well as carbonate species interconversions (Pearson 1986). To ensure stability, the interval was calculated as the smallest of

$$\Delta t = 0.49\frac{\Delta x^2}{nD} \tag{8}$$

or

$$\Delta t = 0.49\frac{K_m}{R_{max}} \tag{9}$$

and then divided by 10. If calculated profiles changed upon an increase in the number of layers, this number was further increased until no change in profiles was observed; however,
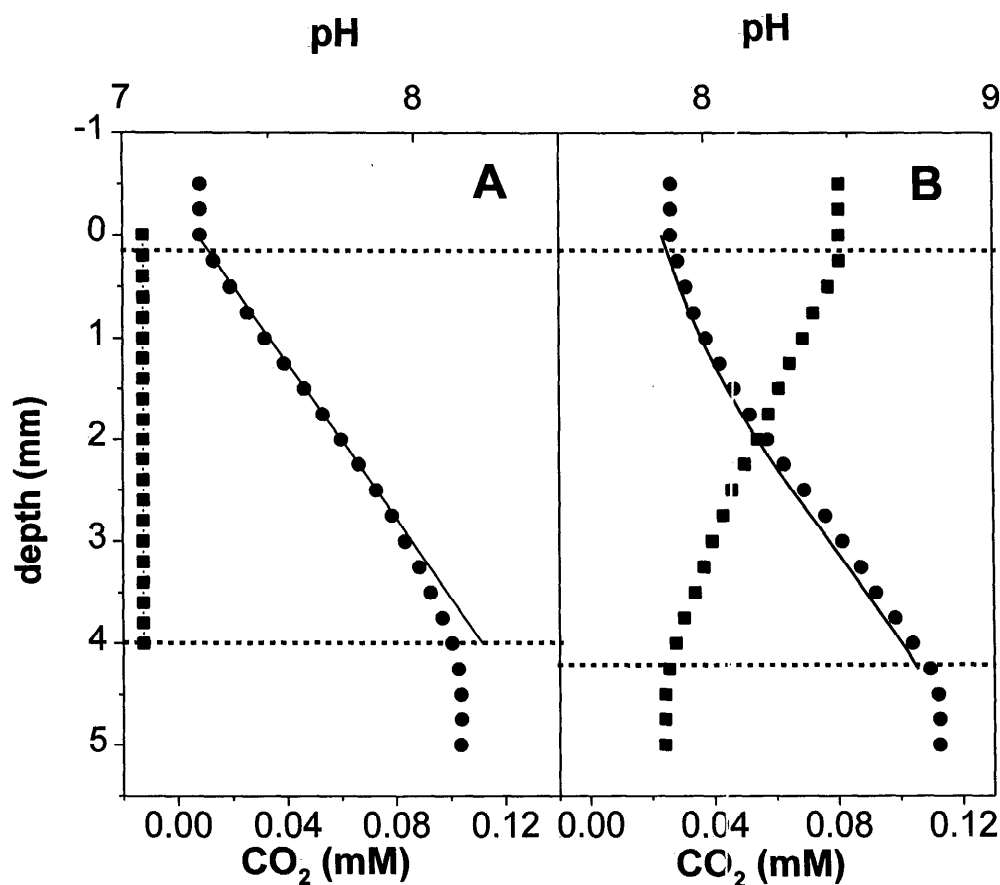
Fig. 4. (A) CO_2 (●—●) and pH (■—■) profiles in an agar slab separating a phosphate buffer with 1 mM sodium carbonate from an identical buffer that was air equilibrated. (B) CO_2 (●—●) and pH (■—■) profiles in an agar slab separating a 4 mM sodium carbonate solution of pH 8.6 and a 5 mM carbonate solution pH 7.8. The continuous lines represent the simulated CO_2 profiles.

the system could only be divided into a maximum number of 180 layers.

For each layer a different set of kinetic parameters can be chosen. Maximum volumetric respiration rates (R_{max}) were estimated by fitting the oxygen profiles with the model. It was assumed that respiration produced CO_2 in stoichiometric amounts from O_2. Similarly, in the agar slab with both respiratory and photosynthetic microorganisms, the net maximum volumetric photosynthesis rate (P_{max}) and R_{max} were estimated from the oxygen profiles. P_{max} was calculated with either CO_2 or both CO_2 and HCO_3^- as substrates for photosynthesis. Photosynthesis was assumed to be absent in the respiratory zone containing *Comamonas*, whereas only photosynthesis was assumed in the photosynthetic zone containing *Synechococcus*. The hydration reactions (Eq. 1 and 4) are slow, while the equilibrium reactions (Eq. 2 and 3) were considered instantaneous (Stumm and Morgan 1981). The values of constants are listed in Table 1.

As initial conditions, the gels and sediments were presumed to be anaerobic and in equilibrium with the carbonate system of the bulk liquid. The calculations were begun by initiating photosynthesis and(or) respiration and(or) by imposing a step change in the oxygen interfacial concentration. Only the profiles inside the porous medium were calculated.

Measured pH profiles were used in all calculations, and microbial growth was not included.

Results

Figure 2 shows examples of calibration curves for CO_2 microsensors with different tip geometries. The signal vs. log[CO_2] plot is not log-linear (Fig. 2A). To visualize the response in the lower CO_2 range, the signal was plotted against the concentration (Fig. 2B). These data were fit with a hyperbolic equation:

$$E = X_1 + \frac{X_2 C}{X_3 + C}, \tag{10}$$

where E is the sensor signal, C the CO_2 concentration, and X_{1-3} constants. These constants were found by iterative least-squares fitting.

The performance of the CO_2 microsensor was influenced strongly by the sensor-tip geometry. The response time (t_{90}) varied between 10 s and a few minutes. All sensors responded ~5 times slower to a decrease than to an increase in CO_2 concentration. If the pH sensor fitted precisely in its casing, high sensitivities (steep calibration slopes) and long response
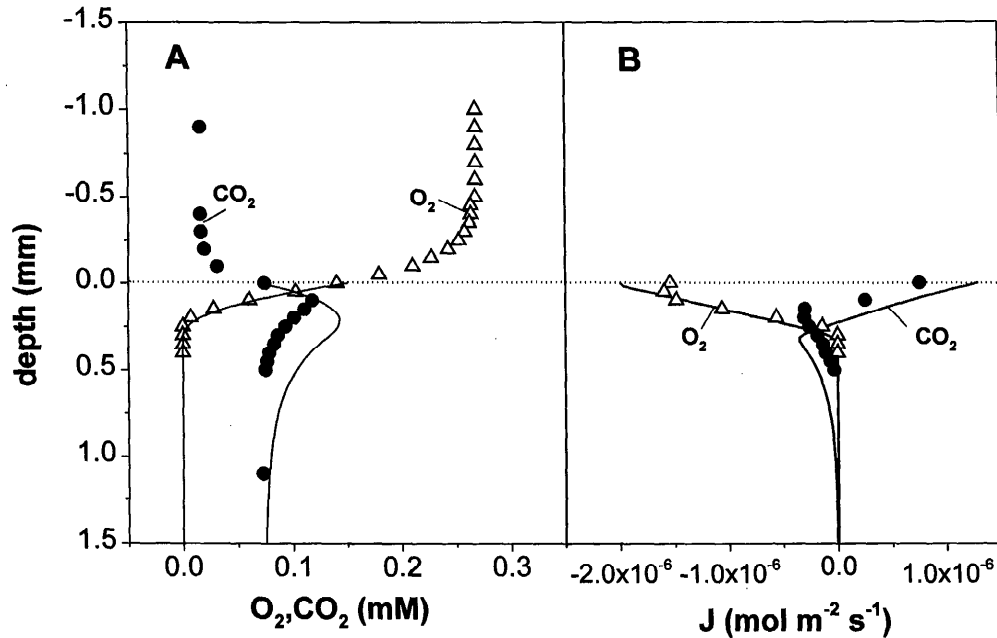
Fig. 5.   (A) CO_2 (●—●) and O_2 (△—△) in an agar slab containing *Comamonas testosteroni*. Continuous lines indicate modeled profiles for CO_2 and O_2. (B) Local fluxes of CO_2 (●—●) and O_2 (△—△). Continuous lines indicate modeled fluxes.

times (>5 min) were observed. The best response times and stabilities were observed for sensors with a loose fit, i.e. with a conical casing and a pH sensor having a tip taper of ~1° over 2 mm. With this tip geometry, the detection limit for CO_2 of a freshly prepared electrode was always <3 μM, the smallest step change used in the calibration procedure. Fresh sensors usually exhibited an initial negative drift that leveled off within 1 h to <3 mV h^{-1}. The experiments reported here were performed with sensors drifting <2 mV h^{-1}. The drift during profiling was estimated by comparing the signal in the bulk solution with its known CO_2 concentration. The drift decreased at lower concentrations: during a 24-h period the signal of an electrode changed 18 mV for 0 mM CO_2 and 45 mV for 1.5 mM CO_2. The drift was not influenced by the measurements themselves.

Omission of carbonic anhydrase led to extremely long response times (>15 min) and reduced detection limits (Fig. 2B). Omission of chloramphenicol led to bacterial growth and deterioration of the sensor response. Good sensors were made with both types of pH LIX. The best results in terms of stability and response times were obtained with pH sensors based on LIX type 1. Upon aging, the sensitivity decreased, while the detection limit and the response time increased. The sensor can be used at least 24 h for CO_2 determinations with a detection limit of <10 μM.

The sensor is rather fragile, as can be expected from a microsensor with a membrane of 5-μm thickness and a tip diameter of 10 μm. However, breakage was rare, and the sensor is sufficiently sturdy for use in sediments, even in coarse sand (data not shown). A damaged silicone membrane can be recognized by a higher sensor signal in degassed water than in air. The electrical resistance of an intact membrane is >100 GΩ; that of a broken membrane decreases to

1–5 MΩ. The electrode was not very sensitive to electrical noise. The signal is sensitive to temperature. A sensor immersed in a 50 mM $NaHCO_3$ solution pH 8.0 (0.112 mM CO_2) showed a signal increase of 0.4 mV per °C between 15 and 41°C (data not shown). No stirring sensitivity was observed. The electrode is in principle sensitive to all gases that have a pH effect upon solution and that can pass the silicon membrane. Indeed, the sensor is very sensitive to H_2S (Fig. 3). However, 45 mM ammonium chloride (pH 8, 2.4 mM NH_3) decreased the signal by only 1 mV.

Microprofile measurements and calculations—In the artificial gradient systems, CO_2 gradients were created by changing the pH and(or) the carbonate concentrations on both sides of an agar slab. The simplest experiment was done with 50 mM phosphate buffer of pH 7.07 to prevent development of a pH gradient. The top chamber was brought in equilibrium with air; the bottom chamber contained 1 mM C_T. No pH gradient developed, and a CO_2 profile could be measured that was almost linear (Fig. 4A). The model results agreed reasonably with the measured values.

In a slightly more complex situation, both pH and C_T gradients were created (Fig. 4B) by placing a 4 mM C_T solution of pH 8.6 on the upper side of the agar membrane and a 5 mM C_T solution of pH 7.7 on the lower side. The pH gradient was measured and used in the reaction-diffusion model to calculate the CO_2 profile, and a good fit was obtained to the measurements.

In agar gels with immobilized microorganisms, both O_2 and CO_2 gradients developed (Fig. 5). O_2 penetrated 250 μm into gels containing *C. testosteroni*. The CO_2 profiles showed a peak in the zone of respiratory activity (Fig. 5A). The interfacial fluxes of CO_2 and O_2, calculated from their pro-
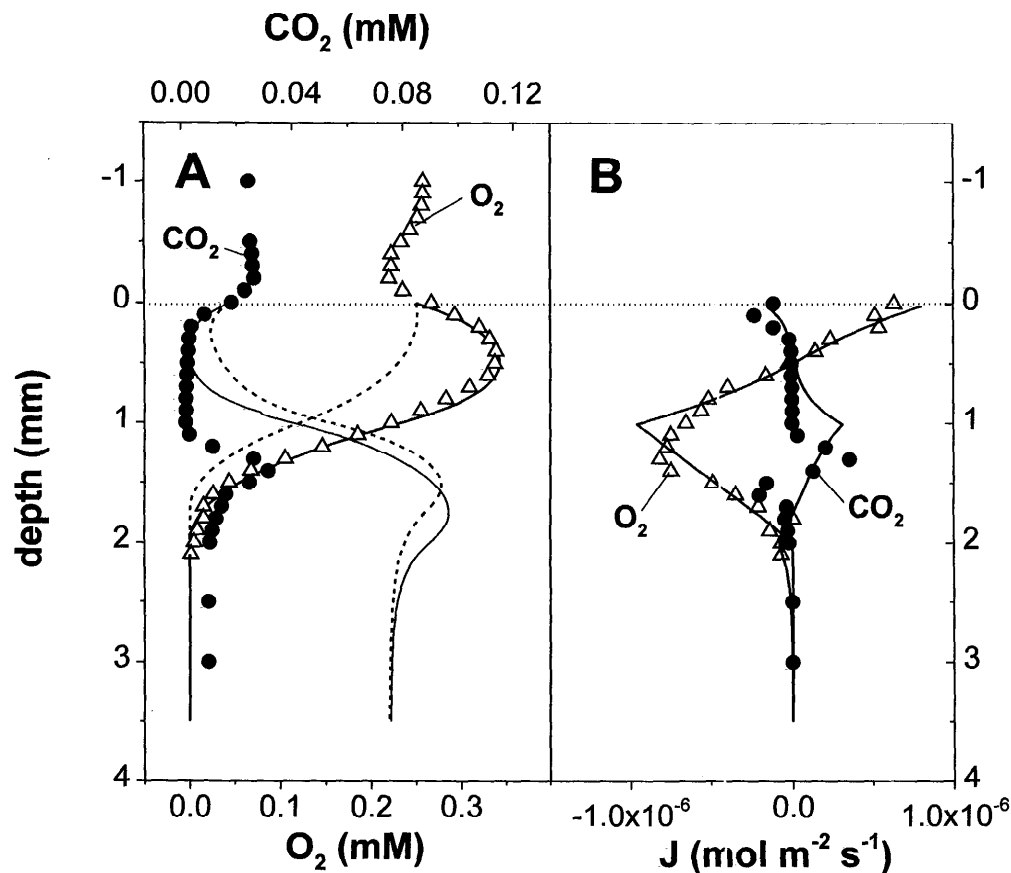
CO$_2$ (mM)

0.00   0.04   0.08   0.12

Fig. 6.   (A) CO$_2$ (●—●) and O$_2$ (△—△) in an agar slab. The bottom part contained *Comamonas testosteroni*; the top layer contained *Synechococcus* spp. Continuous lines indicate modeled profiles for CO$_2$ and O$_2$ assuming that both CO$_2$ and HCO$_2^-$ were substrates for photosynthesis. The dashed line was calculated assuming only CO$_2$ as carbon source for photosynthesis. (B) Measured and modeled local fluxes of CO$_2$ (●—●) and O$_2$ (△—△), modeled profiles are represented by continuous lines. For modeling, both CO$_2$ and HCO$_3$ were assumed substrates for photosynthesis.

files, are of the same order of magnitude but in the opposite direction (Fig. 5B). The pH gradients were not very steep in this system, i.e. a gradual pH decrease was observed of ~0.1 pH unit.

A constant pH value was assumed throughout the agar for modeling CO$_2$ distribution. The O$_2$ profile could be fitted with an R_{max} of 0.007 mol m^{-3} s^{-1}, and using this conversion rate, the CO$_2$ profiles were calculated (Fig. 5A). Only the top 2.5 mm of the 1-cm-thick slab was modeled in order to achieve sufficient spatial resolution in the respiratory zone. According to the model, the oxygen profiles are constant within 20 min; however, steady state for the carbonate system is reached only after 6 h. During this transient state, the agar fills up with C_T, which due to the large size of the pool takes considerable time. According to the model, a CO$_2$ peak will develop.

The transient profiles calculated after 120 min, approximately the incubation time before the profile measurements started, were in reasonable agreement with the measurements; the main difference was that the observed peak was narrower and shifted upward over a distance of 200 μm. Also the local fluxes predicted with the model show reason-

able correspondence with the fluxes calculated from the measured profiles (Fig. 5B).

More complex profiles developed if the *C. testosteroni*-containing gels were covered with a 1-mm gel containing *Synechococcus* and incubated in light (500 μEinst m^{-2} s^{-1}). Photosynthesis induced an O$_2$ peak in the top layer (Fig. 6A). CO$_2$ penetrated into the photosynthetic zone from the bulk liquid and from the gel containing the respiring *C. testosteroni* culture. The respiring culture in turn used the O$_2$ produced by photosynthetic activity in the top layer. CO$_2$ was depleted in the middle of the gel layer containing *Synechococcus*.

The whole agar slab of 1.1-cm thickness could not be simulated with our model. The maximum number of 180 layers was not sufficient to predict accurately the profiles in the most active zones. Therefore, only the top 3.5 mm was modeled. According to the model, steady state should have been achieved after 6 h for a 3.5-mm-thick slab (Fig. 7). Of course, in the 1.1-cm-thick slab used in the experiment, the time to reach steady state was much longer. The buildup of the large C_T pool in the respiratory zone was the main cause of the long time needed to reach steady state. The actual
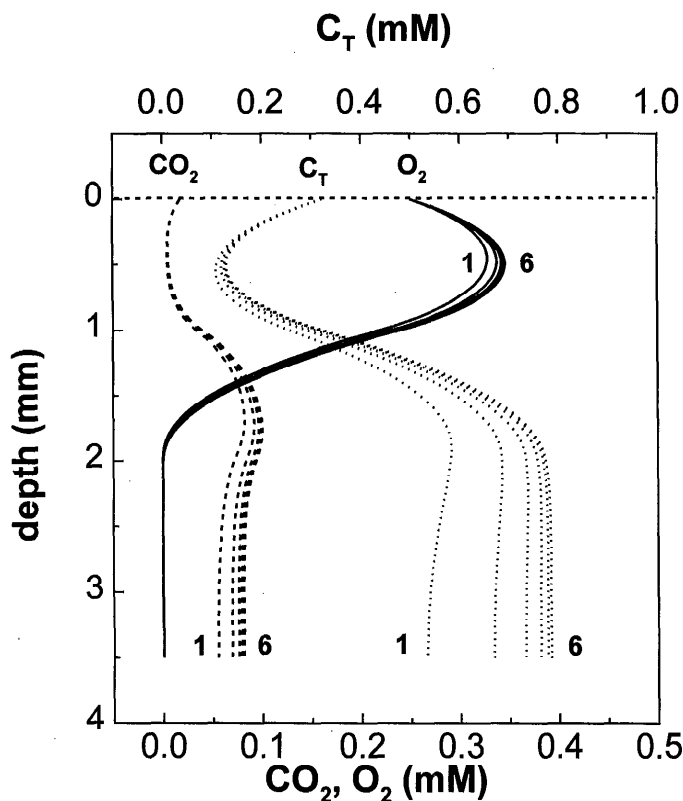
C$_T$ (mM)

Fig. 7. Transient profiles of CO_2 (dashed line), O_2 (solid line), and C_T (dotted line) calculated with the model for the agar slab as described for Fig. 6. Numbers in the graphs indicate the time in hours after start of the simulation.

illumination time was ~2 h; thus, the measurements were most likely not done during steady state. The O_2 profile could be modeled assuming photosynthetic activity throughout the *Synechococcus* containing zone with a P_{max} of 0.002 mol m^{-3} s^{-1} and respiratory activity in the *C. testosteroni*-containing layer with an R_{max} of 0.001 mol m^{-3} s^{-1}. In Fig. 6, the modeled values are given after 2.5 h of incubation. A fit for the O_2 profile could only be obtained if it was assumed that both CO_2 and HCO_3^- were used for photosynthesis. If CO_2 was assumed to be the sole substrate, photosynthesis became CO_2 limited and the oxygen peak in the photosynthetic zone was too small; even if a P_{max} of 0.01 mol m^{-3} s^{-1} was assumed, which is among the highest rates recorded (Jørgensen et al. 1983; Revsbech and Ward 1984), no fit with the oxygen profile could be obtained (data not shown). The shape of calculated CO_2 profiles was similar to the measured profiles, showing a CO_2 peak near the top of the respiratory zone and CO_2 depletion in the photosynthetic zone. However, there was no quantitative agreement. The calculated CO_2 concentration in the respiratory zone was always higher than measured.

The local fluxes of O_2 were 3–4 times higher than those of CO_2 (Fig. 6B). Fluxes calculated from measured and simulated profiles were close, although a precise overlay of the measured and calculated peaks was not achieved.

Finally, the CO_2 microsensor was tested in sediments. In silty sediment, the most prominent changes in O_2, CO_2, and

pH profiles occurred in the top 3 mm (Fig. 8A). O_2 penetrated 3 mm, while the CO_2 profile showed an increase over the same depth interval, below which the profile leveled off. The pH decreased from a value of 8.6 in the water to 7.8 at 3 mm depth, below which it was more or less constant.

Pore-water analysis showed an increase of C_T from 4.25 to ~5.25 mM at a depth of 9 mm, below which it leveled off (Fig. 8B). Using the pH and CO_2 microprofiles and assuming equilibrium, a C_T increase from 3.8 to 5.6 mM was calculated (Fig. 8B). The profiles obtained from pore-water analysis were much less steep than were those obtained with CO_2 and pH microelectrodes. From the measured O_2 profile. R_{max} was calculated (0.0002 mol m^{-3} s^{-1}), and this value was used in the model to calculate the CO_2 profile. For the model calculations the sediment was assumed initially to be anaerobic with a CO_2 concentration equal to that of the overlying waterphase. H_2CO_3, HCO_3, and CO_3^{2-} were assumed to be in equilibrium with the local pH and the CO_2 concentration. $CaCO_3$ dissolution and precipitation were not considered. Only the top 5 mm of the sediment was modeled. The model predicted that a steady state with respect to the CO_2 profile was achieved only after 16 h (data not shown). The calculated C_T concentration inside the sediment reached 4.2 mM.

Discussion

The response of the CO_2 microsensor was not log-linear like that of macrosensors. It is speculated that this is caused by its special tip geometry. Macrosensors are flat plate sensors with a limited internal volume that equilibrates with the CO_2 concentration at the silicon membrane; thus, the proton concentration of the internal electrolyte is directly related to the CO_2 concentration of the sample solution. In contrast, the microsensor is tapered; the internal volume is very large compared to the exchange surface and can be considered infinite. Internally, the microsensor tip approximates a radial diffusion system, with the silicon membrane as a point source or sink for CO_2. The pH in the microsensor tip is then a function of the CO_2 diffusion rate through the membrane, the hydration reaction rate, and the diffusion of protons and CO_2 from the tip into the electrolyte compartment of the electrode casing. It is likely that this dynamic balance leads to the fast response. If the diffusion from the tip to the back of the sensor is limited (sensors with a close fit), a memory effect could be observed. Upon an increase in CO_2, C_T tends to accumulate in the tip with a concomitant large change in pH. A subsequent CO_2 decrease in the sample leads to a slow pH change, because C_T diffusion out of the tip region is restricted. Space between the pH sensor and the casing was needed to allow diffusive exchange of the volume in the very tip of the sensor with the bulk of the electrolyte in the sensor.

The microsensor described here is much faster than the design of Cai and Reimers (1993). This is probably due to the small size, the different tip geometry, and the use of carbonic anhydrase. The addition of carbonic anhydrase to the sensor electrolyte not only decreased the response time significantly, but it also considerably increased the sensitivity and lowered the detection limit. The volumetric activity
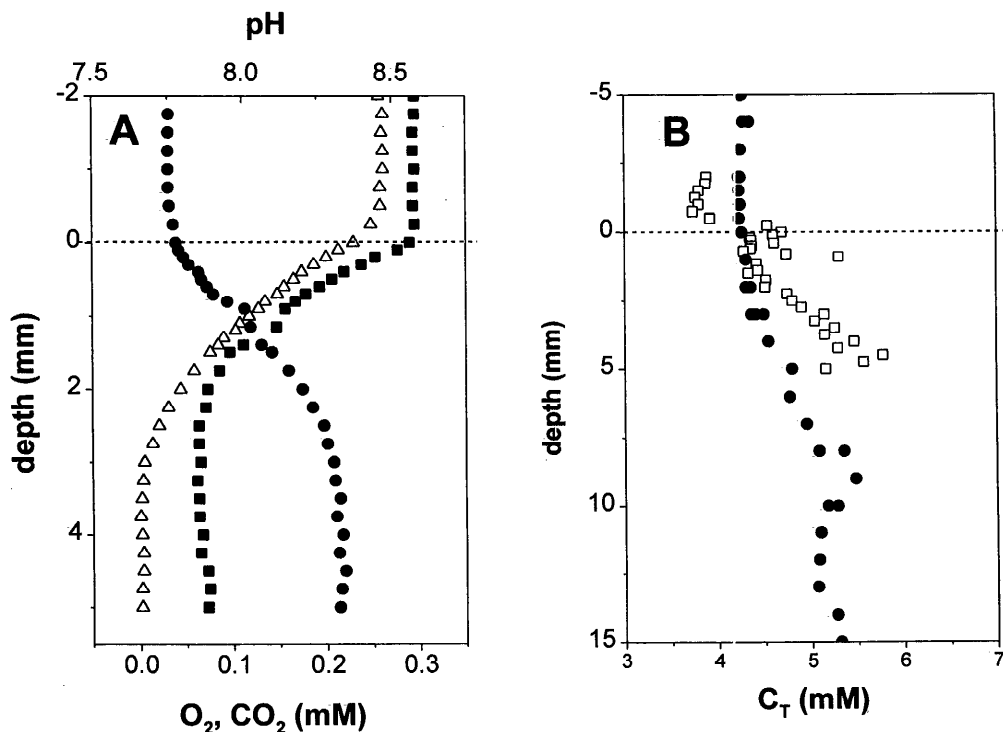
Fig. 8.   (A) CO_2 (●—●), O_2 (△—△), and pH profiles (■—■) in silty sediment. (B) C_T profiles from the same sediments, calculated from the CO_2 and pH microprofiles assuming equilibrium (□—□) and measured by pore-water analysis (●—●).

of carbonic anhydrase solution reaches a plateau at 1 mg ml^{-1} (Ho and Shanahan 1986). We chose a concentration of 5 mg ml^{-1} to compensate for the decrease in enzyme activity.

Ammonia had little effect on the sensor signal. This can be understood from the notion that the sensor responds to the partial pressures of the solutes. At equal concentrations in water the partial pressure of NH_3 is only 0.00059 times that of CO_2 (see Stumm and Morgan 1981), which explains the very small response to ammonium solutions. At equal concentrations the partial pressure of CO_2 is 3 times that of H_2S; therefore, the presence of sulfide will significantly affect the response.

Of importance is whether the measured CO_2 and pH profiles can be used to calculate the other species of the carbonate system. Such a calculation requires an accurate overlay of the pH and the CO_2 profiles. Because the pH profiles are measured separately, the system must be homogeneous in the lateral direction, or the same position must be used for both profile measurements. The determination of the solid–liquid interface may well have an uncertainty of 100 μm. In addition, the pH measurement must be accurate within 0.01 pH unit (Cai and Reimers 1993). Such accuracy is possible with pH microsensors; however, our pH profiles in the agar slabs with microorganisms and sediments varied within 0.1 pH unit. If the overlay between CO_2 and pH profiles is off by 100 μm, the error in the local pH determination may well be 0.1 unit. The calculation of C_T from CO_2 and pH is very sensitive to uncertainties in pH. If, for example, a 0.15 mM CO_2 solution has a pH of 7.8 with an uncertainty of

0.05 units (7.8 ± 0.05), then the calculated C_T will be between 3.9 and 4.9 mM. Thus, the uncertainty is about as large as the maximum DIC difference between water and sediment measured with pore-water extraction. Also in deep-sea studies the problem of lateral variation in pH profiles must be considered; Archer et al. (1989) reported deep-sea profiles measured at one station differing by 0.05 unit. Millero (1995) concluded that calculation of C_T from the CO_2 concentration and pH is the least accurate of all combinations.

Due to the high spatial resolution of the CO_2 microsensor, steep CO_2 gradients can be measured in systems where the carbonate system is out of equilibrium. In those highly active systems, interpretation of the CO_2 profiles is possible only with a reaction-diffusion simulation model. This is illustrated by comparing the model-calculated C_T profiles (the sum of CO_2, H_2CO_3, HCO_3^-, and CO_3^{2-}), C_{Td}, and the C_T profiles derived from the CO_2 profiles assuming local equilibrium (C_{Te}). The ratio of these C_T values is an estimate of the error made in calculating the C_T profiles from measured CO_2 profiles by assuming local equilibrium. As can be seen from Fig. 9, the error made in Exp. 1 (4-mm-thick agar slab with a C_T profile) is negligible, because the gradients are quite gradual. In Exp. 2 (pH and C_T profiles in an agar slab), the error is still small, amounting to <2%. In Exp. 3 (respiratory organism immobilized in agar gel), the gradients are much steeper and the error can be as much as 50%. In Exp. 4, the assumption of local equilibrium leads to a 20-fold underestimation of C_T in the photosynthetic zone and a 40% overestimation in the respiratory zone. Consequently, besides the

In the agar slabs with both respiring and photosynthetic organisms, the model predicted the measured local fluxes. However, the modeled CO_2 concentration in the respiratory zone was overestimated. The measured CO_2 profile reflected a situation after 2–4 h of illumination. This transient state was modeled, although the starting conditions after immobilization are not well known. Moreover, the system was in transient state during the profile measurements; thus, the profiles of the different compounds (O_2, CO_2, pH) must be compared with caution. This suggests that a careful analysis of equilibration times of the carbonate system in natural respiratory-photosynthetic communities is needed.

The CO_2 concentrations measured in sediments were higher than could be expected from aerobic respiration. According to the model, respiration increased the C_T in the sediment by 200 μM. Thus, the measured C_T difference of ~1 mM between the sediment and the overlying water cannot be the result of respiration by oxygen only, as is assumed in the model. In this case, anaerobic mineralization processes probably contribute to the C_T pool. However, Canfield et al. (1993) argued that during aerobic oxidation of products of anaerobic respiration (such as sulfide and methane), the oxygen flux should be close to the C_T flux; thus the C_T gradients should approximately mirror the O_2 gradients. However, a discrepancy between CO_2 and O_2 fluxes has been reported before (Hargrave and Phillips 1981; Rich 1975). Additionally, dissolution of calcium carbonate may have contributed to the large accumulation of dissolved carbonates (Archer et al. 1989; Boudreau 1987). From the comparison of the microelectrode measurements and the pore-water analysis, the spatial resolution of the latter seems not sufficient for the highly active sediments. The pore-water analysis showed a gradient stretching over 9 mm. All measured microprofiles showed major changes in the top 3 mm of the sediment. It must be noted that the steepness of the CO_2 profile in the top 3 mm is caused mainly by the decrease in pH, and much less by an increase in C_T. It is unlikely that all C_T is formed in the aerobic zone; thus, the C_T microprofiles derived from CO_2 and pH profiles may not be reliable.

Due to the slow hydration reaction, the CO_2 gradients become much steeper than they would be if CO_2 instantaneously equilibrated with the much larger C_T pool. Therefore, the slow kinetics of the CO_2 conversion that frustrate the translation of CO_2 profiles to the total carbonate system facilitate visualization of CO_2 converting spots. Although an exact quantification is difficult, conclusions on the state of the carbonate system can be drawn from CO_2 and O_2 profiles in combination with modeling. Photosynthesis in the absence of CO_2 within a microbial mat or algal floc can only be confirmed by direct measurements with the CO_2 microsensor. For example, from a comparison of the O_2 and the CO_2 profile it was concluded that CO_2 could not be the only substrate for photosynthesis in the cyanobacterial biofilm, as O_2 was produced in areas where CO_2 was absent or at least far below K_m for CO_2 uptake (Aizawa and Miyachi 1986). This was also confirmed by modeling the O_2 gradient from the CO_2 and the HCO_3^- gradients. Use of HCO_3^- for photosynthesis is well known in the case of *Synechococcus* and other cyanobacteria (Aizawa and Miyachi 1986), but the new CO_2
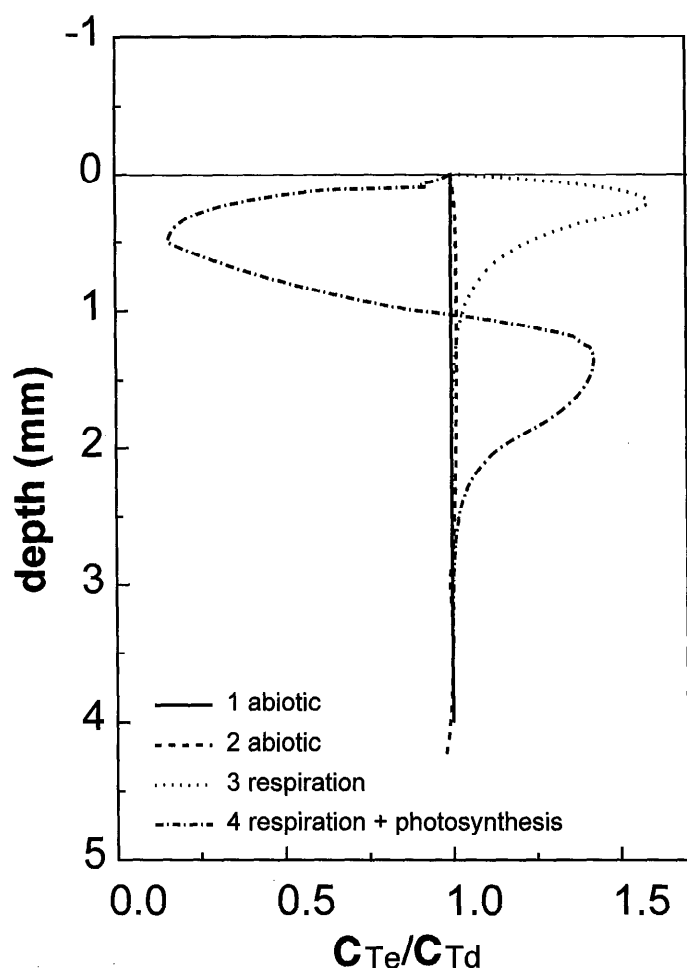

Fig. 9. Estimation of how far the carbonate system was out of equilibrium, using the ratio C_{Te}/C_{Td}. C_{Te} is the total carbonate as determined from the CO_2 and the pH profiles assuming equilibrium, C_{Td} is the total carbonate calculated with the reaction-diffusion model. Given are the estimations for Exp. 1 (Fig. 4A), 2 (Fig. 4B), 3 (Fig. 5), and 4 (Fig. 6).

equilibrium constants and local pH, the kinetics of the hydration reaction must be known and implemented in a diffusion-reaction model in order to calculate carbonate species correctly. The rate constants in water are known; however, in sediments and mats the reaction may be catalyzed to an unknown extent by minerals, biopolymers, and carbonic anhydrase (Stumm and Morgan 1981). Due to the uncertainty of the local pH and the CO_2 hydration kinetics in sediments and microbial mats, extrapolation of CO_2 and pH profiles to C_T profiles must be done with caution.

The presented model was used to examine whether the measured CO_2 profiles were plausible. The program is simple and has limitations. Nevertheless, the model does predict the trends in the CO_2 profiles, even in biological systems. In the experiment with only respiring microorganisms, the measured CO_2 peak was correctly calculated with the model. The correspondence between model and measurement shows that the microsensor is small enough not to disturb the CO_2 profiles.

microsensor can be used in photosynthetic systems where this is not certain.

References

AIZAWA, K., AND S. MIYACHI. 1986. Carbonic anhydrase and CO_2 concentrating mechanisms in microalgae and cyanobacteria. FEMS Microbiol. Rev. **39:** 215–233.

AMMAN, D., T. BÜHRER, U. SCHEFER, M. MÜLLER, AND W. SIMON. 1987. Intracellular neutral carrier-based Ca^{2+} micro-electrode with sub-nanomolar detection limit. Pflügers Arch. **409:** 223–228.

ARCHER, D., S. EMERSON, AND C. REIMERS. 1989. Dissolution of calcite in deep-sea sediments: pH and O_2 micro-electrode results. Geochim. Cosmochim. Acta **53:** 2831–2845.

BENDER, M., W. MARTIN, AND J. HESS. 1987. A whole core squeezer for interfacial pore-water sampling. Limnol. Oceanogr. **32:** 1214–1225.

BOUDREAU, B. P. 1987. A steady-state diagenetic model for dissolved carbonate species and pH in the porewaters of oxic and suboxic sediments. Geochim. Cosmochim. Acta **51:** 1985–1996.

CAI, W.-J., AND C. E. REIMERS. 1993. The development of pH and pCO_2 micro-electrodes for studying the carbonate chemistry of porewater near the sediment–water interface. Limnol. Oceanogr. **38:** 1762–1773.

CANFIELD, D. E., B. B. JØRGENSEN, H. FOSSING, R. GLUD, J. GUNDERSEN, N. B. RAMSING, B. THAMDRUP, J. W. HANSEN, L. P. NIELSEN, AND P. O. J. HALL. 1993. Pathways of organic carbon oxidation in three continental margin sediments. Mar. Geol. **113:** 27–40.

GOYET, C., D. R. WALT, AND P. G. BREWER. 1992. Development of a fiber optic sensor for measurement of pCO_2 in seawater: Design criteria and sea trials. Deep-Sea Res. **39:** 1015–1026.

HALL, P. O. J., AND R. C. ALLER. 1992. Rapid, small volume, flow injection analysis for CO_2 and NH_4^+ in marine and freshwaters. Limnol. Oceanogr. **37:** 1113–1119.

HARGRAVE, B. T., AND G. A. PHILLIPS. 1981. Annual in situ carbondioxide and oxygen flux across a subtidal marine sediment. Estuarine Coastal Shelf Sci. **12:** 725–737.

HERMAN, H. B., AND G. A. RECHNITZ. 1974. Preparation and properties of a carbonate ion-selective membrane electrode. Anal. Chim. Acta **76:** 155–164.

HO, C. S., AND J. F. SHANAHAN. 1986. Carbon dioxide transfer in bioreactors. CRC Crit. Rev. Biotechnol. **4:** 185–252.

JENSEN, K., N. P. REVSBECH, AND L. P. NIELSEN. 1993. Microscale distribution of nitrification activity in sediment determined with a shielded micro-sensor for nitrate. Appl. Environ. Microbiol. **59:** 3287–3296.

JOHNSON, K. S. 1982. Carbon dioxide hydration and dehydration kinetics in seawater. Limnol. Oceanogr. **27:** 849–855.

JØRGENSEN, B. B., N. P. REVSBECH, AND Y. COHEN. 1983. Photosynthesis and structure of benthic microbial mats: Micro-electrode and SEM studies of four cyanobacterial communities. Limnol. Oceanogr. **28:** 1075–1093.

LEE, W., AND D. DE BEER. 1995. Oxygen and pH micro-profiles above corroding mild steel covered with a biofilm. Biofouling **8:** 273–280.

LI, Y.-H., AND S. GREGORY. 1974. Diffusion of ions in sea water and deep sea sediments. Geochim. Cosmochim. Acta **38:** 703–714.

LUDDEN, E., W. ADMIRAAL, AND F. COLIJN. 1985. Cycling of carbon and oxygen in layers mf marine microphytes; a simulation model and its eco-physiological implications. Oecologia **66:** 50–59.

MEHRBACH, C., C. H. CULBERSON, J. E. HAWLEY, AND R. M. PYTKOWICZ. 1973. Measurement of the apparent dissociation constant of carbonic acid in seawater at atmospheric pressure. Limnol. Oceanogr. **18:** 897–907.

MILLERO, F. J. 1995. Thermodynamics of the carbon dioxide system in the oceans. Geochim. Cosmochim. Acta **59:** 661–677.

PEARSON, C. E. 1986. Numerical methods in engineering and science. Van Nostrand Reinhold.

PORTIELJE, R., AND L. LIJKLEMA. 1995. Carbon dioxide fluxes across the air–water interface and its impact on carbon availability in aquatic systems. Limnol. Oceanogr. **40:** 690–699.

REVSBECH, N. P. 1989. An oxygen micro-sensor with a guard cathode. Limnol. Oceanogr. **34:** 474–478.

———, AND D. M. WARD. 1984. Micro-electrode studies of interstitial water chemistry and photosynthetic activity in a hot spring microbial mat. Appl. Environ. Microbiol. **48:** 270–275.

RICH, P. H. 1975 Benthic metabolism of a soft-water lake. Verh. Int. Ver. Limnol. **19:** 440–447.

SEVERINGHAUS, J. W., AND A. F. BRADLEY. 1958. Electrodes for blood P_{O_2} and P_{CO_2} determination. J. Appl. Physiol. **13:** 515–520.

STUMM, W., AND J. J. MORGAN. 1981. Aquatic chemistry, 2nd ed. John Wiley and Sons.